Science and Technology of Advanced Materials

ISSN: 1468-6996 (Print) 1878-5514 (Online) Journal homepage: https://www.tandfonline.com/loi/tsta20

Degradation of high-voltage cathodes for advanced lithium-ion batteries – differential capacity study on differently balanced cells

Philipp Jehnichen, Klaus Wedlich & Carsten Korte

To cite this article: Philipp Jehnichen, Klaus Wedlich & Carsten Korte (2019) Degradation of high-voltage cathodes for advanced lithium-ion batteries – differential capacity study on differently balanced cells, Science and Technology of Advanced Materials, 20:1, 1-9, DOI: 10.1080/14686996.2018.1550625

To link to this article: https://doi.org/10.1080/14686996.2018.1550625

SCIENCE AND TECHNOLOGY OF ADVANCED MATERIALS
2018, VOL. 20, NO. 1, 1–9
https://doi.org/10.1080/14686996.2018.1550625

Taylor & Francis
Taylor & Francis Group

Degradation of high-voltage cathodes for advanced lithium-ion batteries – differential capacity study on differently balanced cells

Philipp Jehnichen, Klaus Wedlich and Carsten Korte

Forschungszentrum Jülich GmbH, Institute for Energy and Climate Research, Jülich, Germany

ABSTRACT

The degradation of $LiNi_{0.5}Mn_{1.5}O_4$ (LNMO) cathodes were investigated using different cell designs (half cells, full cells cathode-limited, anode-limited and cathode-limited with pre-charge). Half cells based on Li/LNMO show long-cycle stability due to the unlimited source of electrochemically available lithium. Full-cell configurations with $Li_4Ti_5O_{12}$/LNMO are limited in their cycling performance and durability. Differential capacity studies during continuous cycling reveal a systematic intensity change of the $Ni^{II/III}$ and $Ni^{III/IV}$ redox peaks as a function of the amount of electrochemically available lithium. As a mechanism, it could be clearly stated that the consumption of electrochemically available lithium determines the cycle stability. The decomposition of the active material itself (e.g. loss of Ni and Mn) is not crucial for the capacity loss. Thus, full cells with a pre-charged anode have the best cycling performance because of its high lithium content.

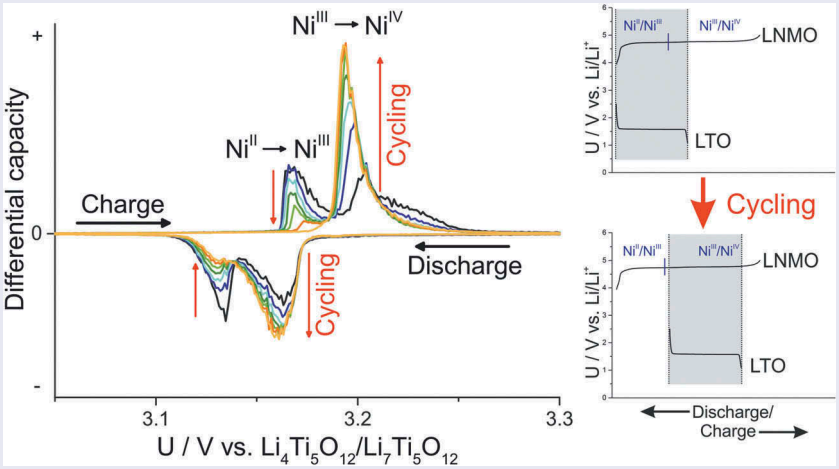

ARTICLE HISTORY
Received 2 May 2018
Revised 16 November 2018
Accepted 17 November 2018

KEYWORDS
High voltage; lithium-ion battery; lithium nickel manganese oxide; energy storage; lithium titanium oxide

CLASSIFICATION
50 Energy Materials; 206 Energy conversion / transport / storage / recovery

1. Introduction

Lithium-ion batteries (LiB) play a highly important role in today's society, being indispensable in the consumer sector and future applications in the transportation sector. Nowadays, most mobile electronic devices are powered by LiB. Therefore, the development of cathode and anode materials to increase the performance and extend the life of batteries is essential. Conventional batteries contain transitional metal oxides with a layer structure, such as $LiCoO_2$ (LCO), $LiNi_{0.33}Mn_{0.33}Co_{0.33}O_2$ (NMC), $LiNi_{0.85}Co_{0.1}Al_{0.05}O_2$ (NCA) or with an olivine structure as in $LiFePO_4$ (LFP). LCO, NMC and NCA have a disadvantage as they contain cobalt, which entails high-production costs. In addition, LCO cathodes are unstable in an exhausted/overcharged state, which is of particular risk for end users [1]. However, LFP cathodes are intrinsically safe, also if overcharged, but have a lower power density than cathodes made with cobaltous compounds. Therefore, efforts have been made to develop new cathode materials with higher energy and power densities. A promising candidate is the spinel-type compound $LiNi_{0.5}Mn_{1.5}O_4$ (LNMO), with a theoretical capacity of 146.7 mAh/g and oxidation plateau of 4.7 V vs. Li/Li^+ [2]. LNMO appears to be a promising successor to conventional-type LiBs with transition metal oxide cathodes and could revolutionize the mobile sector. This cathode material would allow for considerably longer ranges and is cheaper because it does not contain cobalt and is safer under all operating conditions [3]. Unfortunately, LNMO cathodes are subject to severe degradation during charging and discharging [4]. Thus, this cathode material will fail to achieve a commercial breakthrough. There are already

CONTACT Carsten Korte c.korte@fz-juelich.de Forschungszentrum Jülich GmbH, Institute for Energy and Climate Research, IEK-3: Electrochemical Process Engineering, Jülich 52425, Germany
Supplemental material for this article can be accessed here.

numerous publications that deal with the degradation mechanisms of LNMO. In high-voltage batteries, the degradation is largely related to the decomposition of the electrolyte, due to the high potential. A reduction or oxidation of the solvents is possible at the anode and cathode sides [5–9]. An additional performance loss of the LNMO battery is the transition metal dissolution [10]. Jarry et al. postulated a mechanism for the dissolution of the Mn and Ni ions of the LNMO cathode, which forms chelate complexes [11]. Dedryvère et al. demonstrated by X-ray photoelectron spectroscopy measurements that the transition metals migrate to the anode and deposit there [12]. It turns out that a variety of reactions and mechanisms exist and that a combination of all is responsible for the degradation in a battery cell. Nevertheless, there are several approaches to improve the properties of LNMO cathodes; thereby ensuring a lifetime of 5000 cycles. One such approach is the protection of the LNMO particles by coating with TiO_2, $FePO_4$, SnO_2 or Al_2O_3 to prevent direct contact with the liquid electrolyte [13–16]. Furthermore, there are attempts to produce the active material in the form of nanoparticles in order to ensure the largest possible active surface area or that various additives are added to the electrolyte in order to prevent further decomposition of the electrolyte or active material [17–21]. Gabrielli et al. pursued a different approach for longer cycle stability in full cells with silicon/graphite anodes and LNMO cathodes. Employing an overlithiation of LNMO, they were able to compensate the significant capacity loss in the first cycle. However, it is not shown that the continuous degradation, beyond a cycle number of 100 can be stopped, respectively, slowed down, which is accompanied by the use of a high-voltage cathode material [22].

The aim of this work is to understand the mechanism of strong cell degradation after a limited number of cycles. It is shown by means of electrochemical measurements that the main cause of the low cycle stability is the immobilization of the electrochemically active lithium in the cell and not by the degradation of the cathode material itself. In this study, we investigate half cells and full cells with the different balancing of electrochemically available lithium. The evaluation by means of the differential capacity method and the associated voltage characteristics allow a conclusion on the steady reduction of the electrochemically available lithium.

2. Experimental methods

2.1. Electrode preparation

Cathode: The LNMO powder used has an ordered spinel-type structure with the space group $P4_332$. It was purchased from Sigma–Aldrich (725110; USA) and has a particle size of <0.5 μm and purity of >99%. The presence of the ordered phase was confirmed by Raman spectroscopy (Supporting Material) [23]. 85 wt% LNMO, 10 wt% carbon black (CB, Timcal Super C65, Switzerland) and 5 wt% polyvinylidene difluoride (PVdF, Targray D-2, Canada) were mixed in *N*-methylpyrrolidone (NMP, Sigma–Aldrich 99.5%) for 2 h with an *IKA* Ultra Turrax (IKA, Germany) and then doctor-bladed (clearance 150 μm) on aluminum foil. The electrode was dried at 90 °C for 48 h in a vacuum oven.

Anode: The $Li_4Ti_5O_{12}$ (LTO) powder used was purchased from Sigma–Aldrich (702277). The powder has a particle size of <100 nm and purity of >99% (spinel-type structure, space group Fdm). The preparation of the anode is similar to the procedure used for the cathode. 85 wt% LTO, 10 wt% CB and 5 wt% PVdF were mixed in NMP for 2 h and then doctor-bladed (clearance 150 μm) on a copper foil. The electrode was dried at 90 °C for 48 h in a vacuum and stored in an argon-filled glovebox.

2.2. Balancing of the electrodes and electrochemical experiments

For the electrochemical measurements, El-Cell test cells (El-Cell, Germany) were used with a Whatman glass fiber separator (0.65 mm) and LP30 electrolyte, i.e. 1 mol l^{-1} $LiPF_6$ (Sigma–Aldrich, >99.99%) in a 1:1 mixture of ethylene carbonate (EC, Sigma–Aldrich, 99%) and dimethyl carbonate (DMC, Sigma–Aldrich, >99%). Full cells and half cells with various combinations of electrodes with different total capacities and lithiation degrees were assembled. This allows the investigation of cells with different electrochemically balanced cathode–anode combinations, as summarized in Table 1. Disc-shaped LNMO cathodes were punched out with an area of 10 mm^2 (17 mg active mass) and 16 mm^2 (40 mg active mass). For the full cell, LTO anodes with an area of 18 mm^2 were used. In half cells, discs of metallic lithium (area of 16 mm^2, 0.25 mm thickness) were utilized as anodes to provide a (quasi-) unlimited lithium capacity. The cells were cycled with a constant current of 1/2 C. Depending on the initially adjusted cathode and anode capacities and lithiation degrees, different potential ranges had to be used (see Table 1). The electrochemical studies were performed using a Solartron Analytical 1400 Cell Test System (Ametek, USA). For cycling, the cells were placed in a climatic chamber at 23 °C.

3. Results and discussion

3.1. Half cells

Half cells with a lithium anode and LNMO cathode were investigated as a reference for the subsequent study of full cells. In industrial applications, cells with metallic lithium

Table 1. Full and half cells with various cathode–anode capacity balancing.

Name	Anode	Cathode	Balancing	Potential area
Half cell	Metallic Lithium	LNMO (16 mm^2)	No limitation	3.5–5.0 V ~4.7 V Oxidation plateau
Full cell	LTO (18 mm^2)	LNMO (10 mm^2)	Cathode limitation	1.0–3.5 V ~3.2 V Oxidation plateau
Full cell	LTO (18 mm^2)	LNMO (16 mm^2)	Anode limitation	1.0–3.7 V ~3.2 V Oxidation plateau
Full cell	LTO (18 mm^2)	LNMO (10 mm^2)	Cathode limitation with pre-charge	2.0–3.5 V ~3.2 V Oxidation plateau

anodes play only a minor role, because its costs is too high, there is too little cycle stability and it has safety risk due to the potential growth of metallic dendrites [24]. The advantage of a half cell is that lithium can be continuously replenished from the anode, if electrochemically available lithium is immobilized by side reactions, e.g. by forming LiF, Li_2CO_3, $Li_xPF_yO_z$, Li_xPF_y [7]. Figure 1 shows a diagram of the battery's state of health (SoH) and the Coulombic efficiency of a Li/LNMO half cell over 300 cycles. The SoH indicates the level of aging of a battery cell and is calculated from the quotient of the current capacity and capacity of the cell in the first cycle. Since this value is relative, the battery states of different cells with different initial capacities can be compared to one another. The capacity curve of the cell is plotted in Figure 1 as a black line. The capacity decreases slowly but continuously with each cycle. A strong drop in the capacity was not observed. After 300 cycles, the cell still has a SoH of 93.3%. The course of the Coulombic efficiency is represented as a red line. A value of 99% indicates a small fraction of electrochemical side reactions in this cell. In Figure 2, the differential capacitance as a function of the number of cycles is shown (a differential capacity curve for every 60th cycle). During the charging half cycle (delithiation of the cathode), the differential capacity has a positive sign, and a negative sign during the discharging half cycle. In the interest of clarity, only the ranges between 4.5 and 5 V vs. Li/Li^+ are shown for a better overview. The $Ni^{II/III}$ oxidation appears at

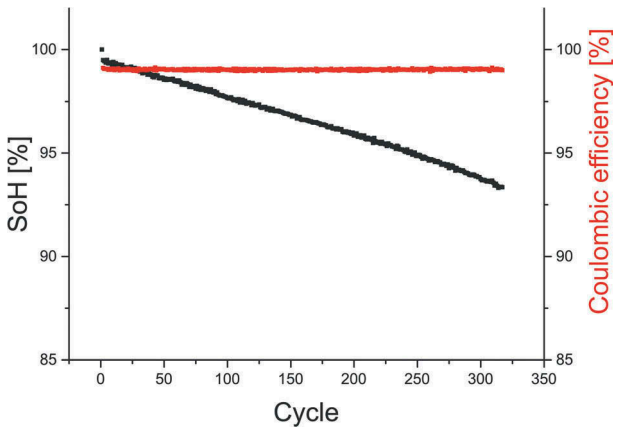

Figure 1. SoH and Coulombic efficiency diagram of 300 cycles of a half cell with LNMO vs. Li/Li^+ and 1 mol $LiPF_6$ DMC:EC solution. Cycled in a range of 3.5–5.0 V vs. Li/Li^+ [30].

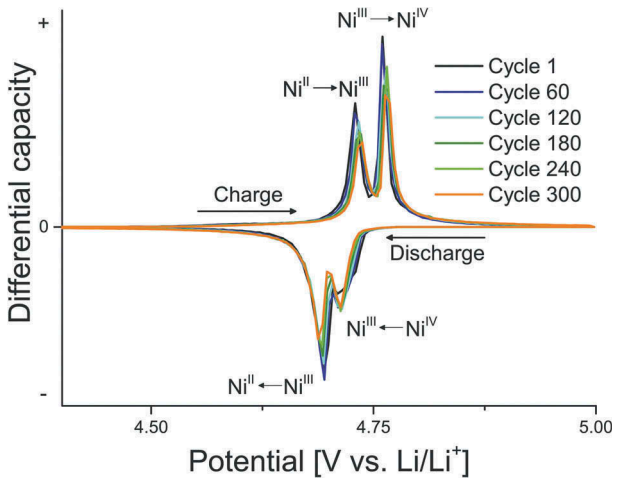

Figure 2. Differential capacity diagram of LNMO vs. Li/Li^+ of 300 cycles with a distribution of 60 cycles. The peaks at 4.73 V Li/Li^+ and 4.76 V vs. Li/Li^+ indicate the oxidation of $Ni^{II/III}$ and $Ni^{II/III}$. At 4.71 V Li/Li^+ and 4.69 V vs. Li/Li^+ is the back reaction to $Ni^{IV/III}$ and $Ni^{III/II}$.

a potential of 4.73 V vs. Li/Li^+ and the $Ni^{III/IV}$ oxidation at 4.76 V vs. Li/Li^+. It can be seen that with increasing numbers of cycles, the integral area of the differential capacity peaks decreases. Over the entire set of cycles, both oxidation stages can be clearly detected, i.e. Ni^{II} is converted to Ni^{III} and subsequently to Ni^{IV} and back. However, there is a shift in the oxidation peaks to a higher voltage and the reduction peaks to a lower voltage. According to Dubarry et al. such a consistent peak shift describes an increase in the (total) cell resistance [25]. The light capacity fade in the half cell configuration can be attributed to two major aspects. On one hand, the transition metals of the cathode are dissolved and migrate to the anode [12] (see Supporting Material). On the other hand, the electrolyte (LP 30) is decomposed and deposes an organic and inorganic layer on the lithium metal [26,27]. As already mentioned, the immobilized lithium can be replaced by lithium from the anode. In the half cell, there is a continuous degradation over 300 cycles, but it is much lower compared to full cells, as described in the next section.

3.2. Full cells

In the literature, a strong capacity loss among LNMO full cells is reported. Therefore, we performed

electrochemical experiments to understand which parameters limit the capacity and determine the degradation rate, respectively. Cells with a cathode limitation, an anode limitation and a cathode-limited cell with a pre-charge were investigated. The different balancing provides information on whether a loss of electrochemically available lithium or the decomposition of the cathode active material is a factor in the total degradation of the cell. The measurements shown here were carried out with ordered LNMO and Whatman® separators. Aktekin et al. and Xiang et al. showed longer cycle stability with disordered LTO/LNMO full cells with Celgard® separators [28,29]. However, the performance of the cells is not priority in this article but the mechanism of the degradation.

3.2.1. Full cells with cathode limitation

In Figure 3, the course of the SoH (black line) and Coulombic efficiency (red line) for a cathode-limited LTO/LNMO full cell are depicted. The battery state of the cell is recorded for over 200 cycles. The irregularity at cycle 75 arose due to a system restart of the potentiostat. In the beginning, within the first 20 cycles, a sharp drop in the capacity was detected, accompanied by a very low Coulombic efficiency. With an increasing number of cycles, the decrease of the capacity slowed down. The Coulombic efficiency increases to 94% within these first 20 cycles. The low value of 94% indicates a large fraction of side reactions in this cell. The reason for these observations could be the connection of the capacity loss to the side reactions in the battery. The cell is cycled with a constant current. The capacity decrease and the C rate increases. The residence time at extreme electrode potentials and thus the extent to which the side reactions occur decreases. The Coulombic efficiency of the cell also decreases due to the increasing C rate. The differential capacity of the cell is shown in Figure 4. In Figure 4(a), the first 20 cycles of the cell with a resolution of three cycles are plotted while in Figure 4(b) the following 120 cycles with a resolution of 20 cycles are indicated. In the first 20 cycles, both redox processes, $Ni^{II/III}$ and $Ni^{III/IV}$, can be observed. The first oxidation peak appears at a potential of 3.17 V vs. Li/Li^+ and the second at a potential of 3.2 V vs. Li/Li^+. The area of the peak attributed to $Ni^{II/III}$ oxidation does not change during the first 20 cycles. However, the area of the peak attributed to the $Ni^{II/III}$ oxidation decreases considerably across these. Between the 16th and 19th cycle, the peak has completely vanished and the corresponding redox reaction no longer corresponds to the total cell capacity. Beyond the 20th cycle, the peak of $Ni^{III/IV}$ oxidation starts to lose intensity. Beyond the 140th cycle, no redox peak can be detected in the differential capacity graph, resulting in a complete loss of the cell's capacity. LNMO undergoes two phase transitions with increasing delithiation (charge of the cell). First, in the fully lithiated phase, $LiNi^{II}_{0.5}Mn^{IV}_{1.5}O_4$ Ni^{II} is oxidized into Ni^{III}, resulting in a half-delithiated phase $Li_{0.5}Ni^{III}_{0.5}Mn^{IV}_{1.5}O_4$ and, subsequently, to Ni^{IV}, which ends up in a (nearly) fully delithiated phase, $Ni^{IV}_{0.5}Mn^{IV}_{1.5}O_4$. The capacity loss of the cathode-limited cell during the first 20 cycles is accompanied by the fading of the redox peaks, corresponding to the phase transition between the fully- and half-lithiated phase, may be caused by the gradual loss of electrochemically available lithium. The cathode active material can no longer be completely lithiated and the amount of the fully lithiated phase decreases with an increasing number of cycles. Beyond the 20th cycle, the fully lithiated phase can no longer be achieved. Subsequently, due to the ongoing lithium loss, as well as the second redox peak, the phase transition between the half- and fully delithiated phase also begins to shrink. Degradation (decomposition) of the cathode active material itself can also cause a total capacity loss of the cell, but this should result in the simultaneous fading of both redox peaks in the differential capacity plot with an increasing number of cycles. This was not observed though.

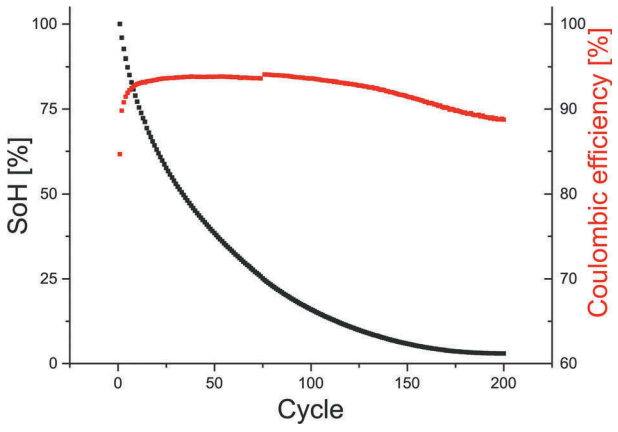

Figure 3. SoH and Coulombic efficiency diagram of 200 cycles of a cathode-limited full cell with LNMO vs. LTO and 1 mol $LiPF_6$ DMC:EC solution. Cycled in a range of 1.0–3.5 V vs. Li/Li^+.

This observation can be clarified by considering the voltage characteristics of both electrodes, i.e. by plotting the charge/discharge curves of the electrodes (electrode potential vs. the charging state of the cell), as shown in Figure 4(c–e). The state in the first cycle is depicted in Figure 4(c), while the state in the 20th cycle is in Figure 4(d) and that beyond the 140th cycle in Figure 4(e). The two areas of the phase transformations of the LNMO are separated by a blue line. The shaded areas indicate the involved part of the cell during the cyclization process.

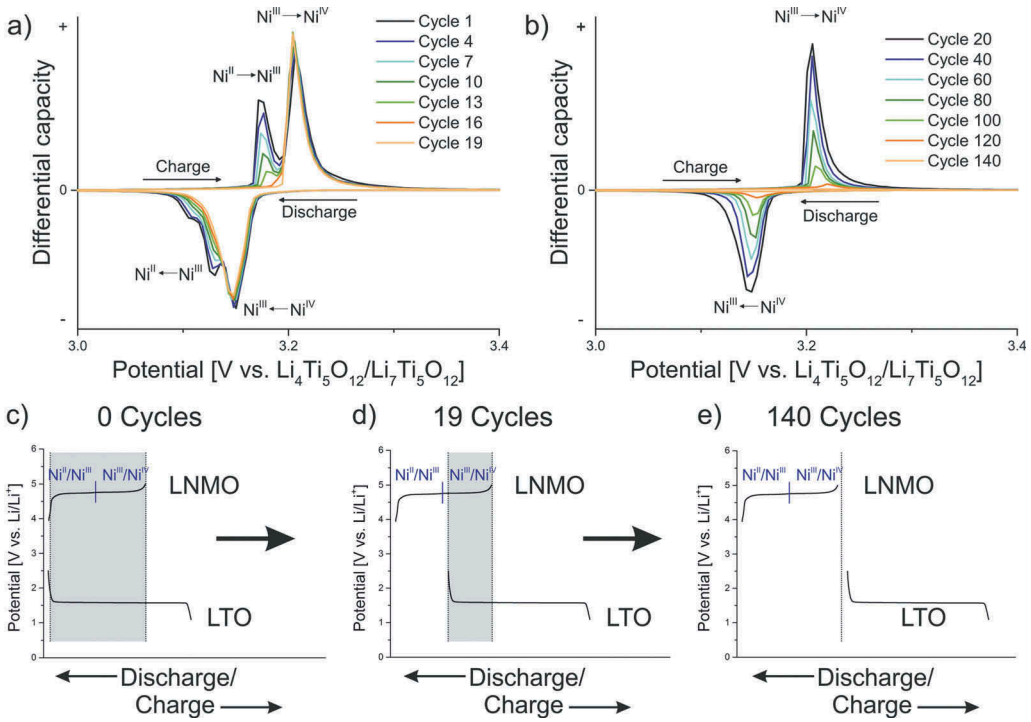

Figure 4. Development of the differential capacity of a cathode-limited full cell with LNMO vs. LTO. (a) First 20 cycles of the cell; (b) the following 120 cycles; (c–e) the corresponding shift of the voltage characteristics of the electrodes to each other. The blue line separates the regions of the two-phase transformations of the LNMO. The gray area between the dashed lines marks the amount of lithium left in the cell.

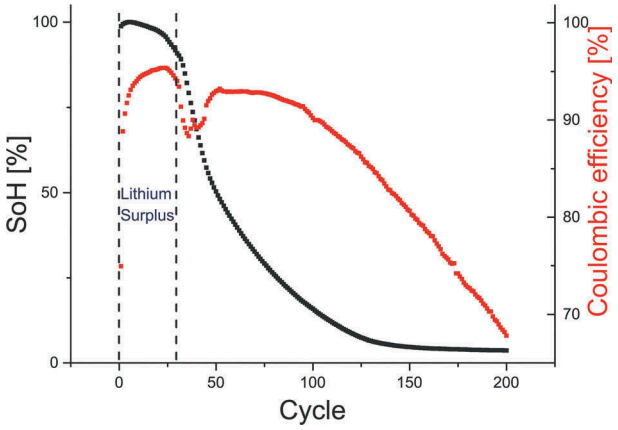

Figure 5. SoH and Coulombic efficiency diagram of 200 cycles of an anode-limited full cell with LNMO vs. LTO and 1 mol $LiPF_6$ DMC:EC solution. Cycled in a range of 1.0–3.7 V vs. Li/Li^+.

If electrochemically available lithium is immobilized in the cell, the cathode material is no longer completely lithiated, but the anode material remains completely delithiated. As a result, the charge/discharge curves of the electrodes shift against each other. The amount of the fully lithiated phase of LNMO, which can be formed, grows smaller. In Figure 4(d), the curves have shifted so far that the end-of-charge voltage is already reached before the cathode material converts to the fully lithiated phase. This corresponds to approximately the 20th cell cycle. After this, the completely delithiated phase of the material is only transformed to the partially lithiated phase. If the charge/discharge curves continue to shift, less and less of the half-lithiated phase is formed during the cycles. Figure 4(e) shows the extreme case, in which the complete electrochemically available lithium is immobilized in the cell and both electrode materials are only present in their fully delithiated state. This case occurs beyond the 140th cycle of the cell.

3.2.2. *Full cells with anode limitation*

In Figure 5, the cyclization of a full cell with anode limitation is shown. In cases with the anode limitation, there is an excess of electrochemically available lithium. The capacity of the cathode exceeds that of the anode. Thus, the cathode cannot be completely delithiated at the beginning of the cyclization. The red curve corresponds to the Coulombic efficiency while the black curve corresponds to the battery state (SoH). The behavior of the anode-limited cells in the beginning is very similar to that of the cathode-limited cells. In the first cycle, the Coulombic efficiency also shows only very low values. After about 10 cycles, it rises to 95%. Unlike the cathode-limited cells, the SoH curve plateaus from the beginning up to the 30th cycle. In Figure 5, this range is marked by dashed lines. At the end of the plateau, a strong loss of capacity appears, as the Coulombic efficiency drops by 7%, recovers to 93% and then decreases steadily as the number of cycle increases.

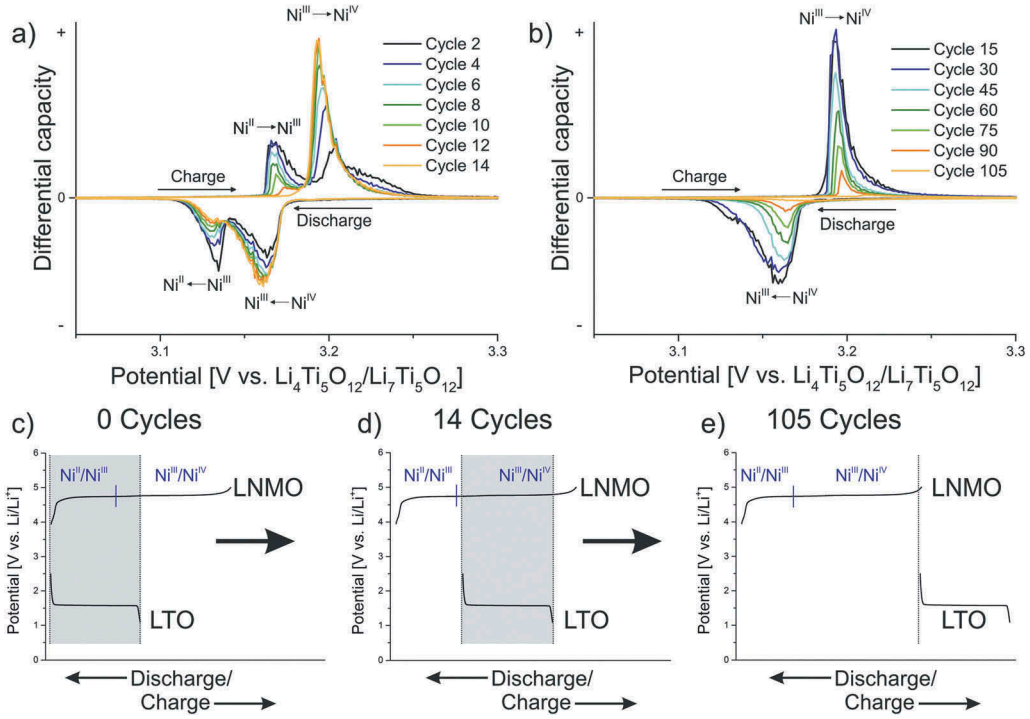

Figure 6. Development of the differential capacity of an anode-limited full cell with LNMO vs. LTO. (a) First 14 cycles of the cell; (b) the following 90 cycles; (c–e) the corresponding shift of the voltage characteristics of the electrodes to each other. The blue line separates the regions of the two-phase transformations of the LNMO. The gray area between the dashed lines marks the amount of lithium left in the cell.

In Figure 6(a) and (b), the differential capacity for a cell with anode-limitation is shown. The first 14 cycles of the cell are depicted with a resolution of two cycles and the following 90 cycles with a resolution of 15 cycles. Analogous to the observation in the cathode-limited cell, the $Ni^{II/III}$ peak decreases strongly within the first 10 cycles and is completely gone by the 14th cycle. However, the behavior of the $Ni^{III/IV}$ redox peaks differs completely from previous observations. These redox peaks increase within the first number of cycles and reach their maximum intensity with the 15th cycle. The peak intensity remains constant between the 15th and 30th cycles. Beyond the 30th cycle, the intensity of the $Ni^{III/IV}$ redox peaks is also decreasing, accompanied by a decrease in the capacity as in the cathode-limited cells.

The plateau at the beginning, between the start and 30th cycle, may result from the excess capacity of the cathode relative to the anode, i.e. an excess of electrochemically available lithium. This can be illustrated by the voltage characteristics of this cell in Figure 6(c–e). Figure 6(c) shows the initial state of the cell. The LTO anode can be completely lithiated while charging the cell, while the LNMO cathode is only partially delithiated. The half-delithiated LNMO phase only partially transforms into the completely delithiated phase (see Figure 6(c)). Thus, in the beginning the corresponding $Ni^{III/IV}$ redox peaks are only small. If the immobilization of lithium due to side reactions is responsible for the capacity loss, the excess of electrochemically available lithium must first be consumed before a significant capacity drop can be observed. The charge/discharge curves of the electrodes in the voltage characteristics shift against each other with each cycle. This should result in an initial plateau for the SoH curve. The intensity of the $Ni^{III/IV}$ redox peaks will increase and, correspondingly, the intensity of the $Ni^{II/III}$ redox peaks will decrease within the first 14 cycles. From the beginning of the 14th cycle, the fully lithiated phase is no longer formed (see Figure 6(d)). From this cycle to the 30th, only the half and delithiated phases are formed. Since the LTO anode is still completely lithiated and delithiated at each cycle, the capacity of the cell does not change in the first 30 cycles. Beyond the 30th cycle, the amount of electrochemically available lithium in the cell is so low that even the LTO anode can no longer be completely lithiated. Thus, its charge/discharge curve in the voltage characteristic is only partially below the curve of the cathode and the lithiation decreases with each additional cycle. The final, fully exhausted state is reached by the 105th cycle, as shown in Figure 6(e). The curves no longer overlap and both electrode materials are only present in their almost completely delithiated state.

3.2.3. *Full cells with cathode limitation and pre-charging*

Comparing the differential capacity plots and cycling behavior of the cathode- and anode-limited cells suggests that the total amount of electrochemically

available lithium is crucial for the onset of the drastic capacity fade. Experiments with cathode-limited cells were performed to justify this assumption. An excess of electrochemical lithium was introduced by constructing a cell with an LTO anode that was previously lithiated using a half cell setup (pre-charge). Figure 7 shows the cycling stability for a full cell with cathode limitation and anode pre-charge. In this cell configuration, a plateau appears during the first 40 cycles, as is observed for the anode-limited cells. This range is marked by dashed lines. Once again, at the end of the plateau a strong loss of capacity appears. However, in comparison to the anode-limited cells, the capacity decrease is less rapid. The Coulombic efficiency also shows more stability than the other cell setups. In the range of the plateau it reaches a maximum of 96%, and during the subsequent strong loss of capacity reduces to a value of about 94%. With an increasing number of cycles, it decreases very slowly.

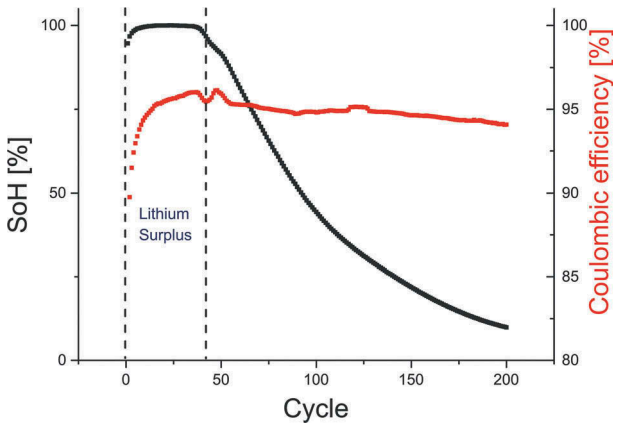

Figure 7. SoH and Coulombic efficiency diagram of 200 cycles of an anode pre-charged full cell with LNMO vs. LTO and 1 mol $LiPF_6$ DMC:EC solution. Cycled in a range of 2.0–3.5 V vs. Li/Li^+.

Figure 8 shows the cycling behavior of differential capacity from the first to the 160th cycle. There is virtually no substantial change in intensity for the $Ni^{II/III}$ and $Ni^{III/IV}$ redox peaks within the first 50 cycles. Beginning with the 50th cycle, the intensity of the $Ni^{II/III}$ redox peaks begins to decrease. In the meantime, the intensity of the $Ni^{III/IV}$ redox peaks does not change. Beyond the 91st cycle, the intensity of the $Ni^{III/IV}$ redox peaks also start to decrease and that of the $Ni^{II/III}$ redox peaks completely fade out. Beyond the 160th cycle, no noteworthy capacity remains.

The observed cycling behavior can again be explained by the shifts of the charge/discharge curves of the electrodes during the cycling in the voltage characteristics (see Figure 8(c–e)). In first cycles, the charge/discharge curves of the cathode are shifted far to the right of the charge/discharge curve of the anode due to the pre-charge. Despite the continuous loss of electrochemically available lithium, during the first 50 cycles the amount is sufficient for the complete lithiation of the cathode material. This results in a nearly constant SoH, i.e. the observed plateau. At the end of the 50th cycle, the remaining quantity of

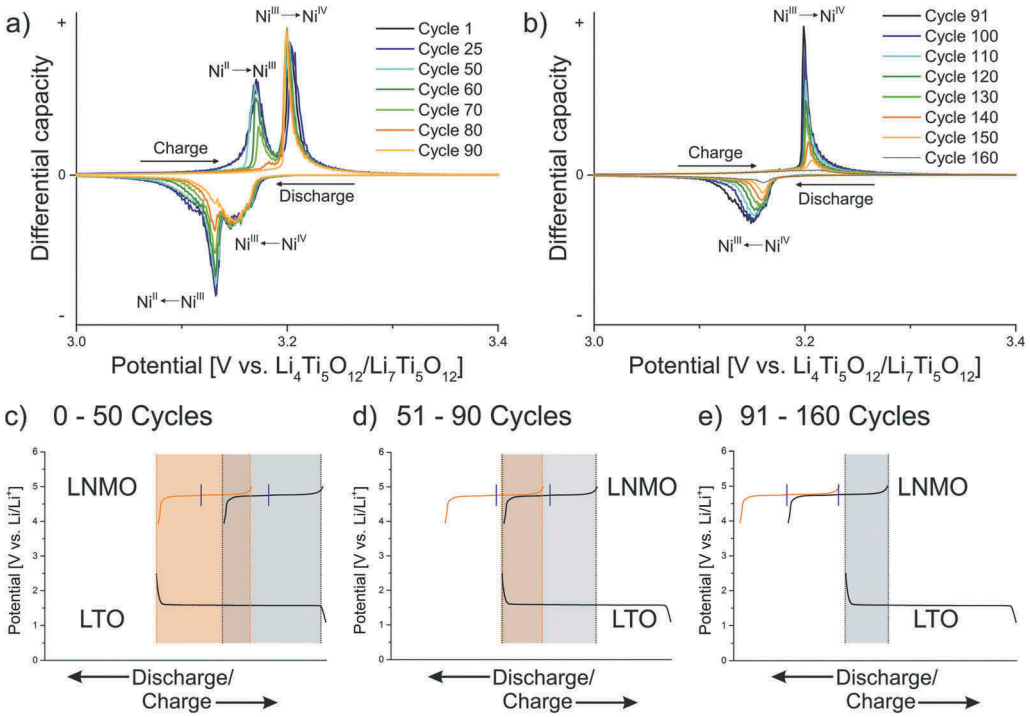

Figure 8. Development of the differential capacity of a cathode-limited full cell with a pre-charged anode with LNMO vs. LTO. (a) First 90 cycles of the cell; (b) the following 70 cycles; (c–e) the corresponding displacement of the voltage characteristics of the electrodes to each other. The blue line separates the regions of the two-phase transformations of the LNMO.

electrochemically available lithium corresponds to the capacity of the cathode. After the 50th cycle, the cell behaves like a cathode-limited cell, because the pre-charge surplus of electrochemically available lithium is completely bound, as depicted in Figure 8(d). In the following cycles, the immobilization of the electrochemically available lithium proceeds. Due to the ongoing shifting of the charge/discharge curve of the cathode and anode, the fraction of the fully lithiated LNMO phase, which is formed in a cycle, decreases continuously (see Figure 8(d)). After the 90th cycle, the fully lithiated LNMO phase is no longer formed and also, the intensity of the $Ni^{III/IV}$ redox peaks also begins to decrease (see Figure 8(e)). Beyond the 160th cycle, all the electrochemically available lithium in the cell is bound and the electrodes are (nearly) in the fully delithiated state. No capacity is left. The findings on cathode-limited cells with pre-charge anodes correspond to the behavior of the other investigated cell setups and confirm the assumption that only the loss of the electrochemically available lithium determines the rate of cell degradation. The decomposition of the cathode material itself may only have a minor impact.

4. Conclusions

In the present work, the high-voltage cathode material LMNO was investigated. Using cell setups differentially balanced between the cathode and anode capacity, the influence of the electrochemically available lithium in the cell on the degradation rate could be investigated. The observed courses of the SoH as a function of cycles and the change in the differential capacity can only be explained by the steady immobilization of the electrochemically available lithium in the cell. The lithium is bound in the battery by side reactions (oxidation processes with the solvent) and is thus no longer available for the lithiation of the electrodes. From the comparison with the half cell and full cell, it is made clear that the degradation of the cathode material is not caused by the loss by Ni or Mn ions from the cathode material. Thus, the cathode material is not irreversibly decomposed by the side reactions with the solvent, leading to the immobilization of lithium and the steady self-discharge of the cell. These experiments clearly identified the immobilization of the electrochemically available lithium in the cell as a responsible mechanism for the large capacity loss of $LiNi_{0.5}Mn_{1.5}O_4$ full cells. Furthermore, due to the steady loss of electrochemically available lithium, it can be concluded that a stable, protective layer does not form on the cathode material.

Disclosure statement

No potential conflict of interest was reported by the authors.

Funding

We want to thank the Helmholtz Association for their financial support.

ORCID

Philipp Jehnichen http://orcid.org/0000-0002-8665-1650
Carsten Korte http://orcid.org/0000-0001-6574-6223

References

[1] Doughty DH, Pesaran AA. Vehicle battery safety roadmap guidance. National Renewable Energy Laboratory, U.S. Department of Energy; 2012. Report No. NREL/SR-5400-54404.
[2] Takahashi K, Saitoh M, Sano M, et al. Electrochemical and structural properties of a 4.7 V-class $LiNi_{0.5}Mn_{1.5}O_4$ positive electrode material prepared with a self-reaction method. J Electrochem Soc. 2004;151(1):A173.
[3] Ma J, Hu P, Cui G, et al. Surface and interface issues in spinel $LiNi_{0.5}Mn_{1.5}O_4$: insights into a potential cathode material for high energy density lithium ion batteries. Chem Mater. 2016;28(11):3578–3606.
[4] Lu D, Xu M, Zhou L, et al. Failure mechanism of graphite/$LiNi_{0.5}Mn_{1.5}O_4$ cells at high voltage and elevated temperature. J Electrochem Soc. 2013;160(5):A3138–A3143.
[5] Aurbach D, Markovsky B, Salitra G, et al. Review on electrode–electrolyte solution interactions, related to cathode materials for Li-ion batteries. J Power Sources. 2007;165(2):491–499.
[6] Tasaki K. Solvent decompositions and physical properties of decomposition compounds in Li-ion battery electrolytes studied by DFT calculations and molecular dynamics simulations. J Phys Chem A. 2005;109:2920–2933.
[7] Yang L, Ravdel B, Lucht BL. Electrolyte reactions with the surface of high voltage $LiNi_{0.5}Mn_{1.5}O_4$ cathodes for lithium-ion batteries. Electrochem Solid State Lett. 2010;13(8):A95.
[8] Duncan H, Abu-Lebdeh Y, Davidson IJ. Study of the cathode–electrolyte interface of $LiNi_{0.5}Mn_{1.5}O_4$ synthesized by a sol–gel method for Li-Ion batteries. J Electrochem Soc. 2010;157(4):A528.
[9] Michalak B, Berkes BB, Sommer H, et al. Gas evolution in $LiNi_{0.5}Mn_{1.5}O_4$/graphite cells studied in operando by a combination of differential electrochemical mass spectrometry, neutron imaging, and pressure measurements. Anal Chem. 2016;88(5):2877–2883.
[10] Pieczonka, NPW, Liu Z, Lu P, et al. Understanding transition-metal dissolution behavior in $LiNi_{0.5}Mn_{1.5}O_4$ high-voltage spinel for lithium ion batteries. J Phys Chem C. 2013;117(31):15947–15957.
[11] Jarry A, Gottis S, Yu Y-S, et al. The formation mechanism of fluorescent metal complexes at the $Li_xNi_{0.5}Mn_{1.5}O_{4-\delta}$/carbonate ester electrolyte interface. J Am Chem Soc. 2015;137(10):3533–3539.
[12] Dedryvère R, Foix D, Franger S, et al. Electrode/electrolyte interface reactivity in high-voltage spinel $LiNi_{0.5}Mn_{1.6}O_4$/$Li_4Ti_5O_{12}$ lithium-ion battery. J Phys Chem C. 2010;114:10999–11008.
[13] Xiao B, Leontiadou MA, Page R, et al. Unravelling the role of electrochemically active $FePO_4$ coating by

atomic layer deposition for increased high-voltage stability of $LiNi_{0.5}Mn_{1.5}O_4$ cathode material. Adv Sci. 2015;2(5).
[14] Sun P, Ma Y, Zhai T, et al. High performance $LiNi_{0.5}Mn_{1.5}O_4$ cathode by Al-coating and Al^{3+}-doping through a physical vapor deposition method. Electrochim Acta. 2016;191:237–246.
[15] Ma F, Geng F, Yuan A, et al. Facile synthesis and characterization of a SnO_2-modified $LiNi_{0.5}Mn_{1.5}O_4$ high-voltage cathode material with superior electrochemical performance for lithium ion batteries. Phys Chem Chem Phys. 2017;19(15):9983–9991.
[16] Tao S, Kong F, Wu C, et al. Nanoscale TiO_2 membrane coating spinel $LiNi_{0.5}Mn_{1.5}O_4$ cathode material for advanced lithium-ion batteries. J Alloys Compd. 2017;705:413–419.
[17] Lee TJ, Lee JB, Yoon T, et al. Tris(pentafluorophenyl) silane as an electrolyte additive for 5 V $LiNi_{0.5}Mn_{1.5}O_4$ positive electrode. J Electrochem Soc. 2016;163(6): A898–A903.
[18] Haregewoin AM, Wotango AS, Hwang B-J. Electrolyte additives for lithium ion battery electrodes: progress and perspectives. Energy Environ Sci. 2016;9(6):1955–1988.
[19] Xu J, Xia Q, Chen F, et al. Facilely solving cathode/electrolyte interfacial issue for high-voltage lithium ion batteries by constructing an effective solid electrolyte interface film. Electrochim Acta. 2016;191:687–694.
[20] Yi T-F, Mei J, Zhu Y-R. Key strategies for enhancing the cycling stability and rate capacity of $LiNi_{0.5}Mn_{1.5}O_4$ as high-voltage cathode materials for high power lithium-ion batteries. J Power Sources. 2016;316:85–105.
[21] Mancini M, Axmann P, Gabrielli G, et al. A high-voltage and high-capacity $Li_{1+x}Ni_{0.5}Mn_{1.5}O_4$ cathode material: from synthesis to full lithium-ion cells. ChemSusChem. 2016;9(14):1843–1849.
[22] Gabrielli G, Marinaro M, Mancini M, et al. A new approach for compensating the irreversible capacity loss of high-energy Si/C|$LiNi_{0.5}Mn_{1.5}O_4$ lithium-ion batteries. J Power Sources. 2017;351:35–44.
[23] Boulet-Roblin L, Villevieille C, Borel P, et al. Versatile approach combining theoretical and experimental aspects of Raman spectroscopy to investigate battery materials: the case of the $LiNi_{0.5}Mn_{1.5}O_4$ spinel. J Phys Chem C. 2016;120(30):16377–16382.
[24] Xu K. Nonaqueous liquid electrolytes for lithium-based rechargeable batteries. Chem Rev. 2004;104(10):4303–4417.
[25] Dubarry M, Svoboda V, Hwu R, et al. Incremental capacity analysis and close-to-equilibrium OCV measurements to quantify capacity fade in commercial rechargeable lithium batteries. Electrochem Solid State Lett. 2006;9(10):A454.
[26] Aurbach D, Ein-Ely Y, Zaban A. The surface chemistry of lithium electrodes in alkyl carbonate solutions. J Electrochem Soc. 1994;141(1).
[27] Aurbach D, Moshkovich M, Cohen Y, et al. The study of surface film formation on noble-metal electrodes in alkyl carbonates/Li salt solutions, using simultaneous in situ AFM, EQCM, FTIR, and EIS. Langmuir. 1999;15:2947–2960.
[28] Aktekin B, Younesi R, Zipprich W, et al. The effect of the fluoroethylene carbonate additive in $LiNi_{0.5}Mn_{1.5}O_4$–$Li_4Ti_5O_{12}$ lithium-ion cells. J Electrochem Soc. 2017;164(4):A942–A948.
[29] Xiang HF, Zhang X, Jin QY, et al. Effect of capacity matchup in the $LiNi_{0.5}Mn_{1.5}O_4/Li_4Ti_5O_{12}$ cells. J Power Sources. 2008;183(1):355–360.
[30] Wedlich K. Investigation of the formation of surface layers on $LiNi_{0.5}Mn_{1.5}O_4$-high-voltage-cathodes: the cathode/electrolyte interface of high-voltage-lithium-ion-batteries. Dissertation, RWTH Aachen. 2017;381:89.